Static dipole polarizability of hydrogenlike ions in Debye plasmas

Y. Y. Qi,[1,2] J. G. Wang,[2] and R. K. Janev[3]
[1]*School of Electrical Engineering, Jiaxing University, Jiaxing 314001, China*
[2]*China Laboratory of Computational Physics, Institute of Applied Physics and Computational Mathematics, P.O. Box 8009-26, Beijing 100088, China*
[3]*Macedonian Academy of Sciences and Arts, P.O. Box 428, 1000 Skopje, Macedonia*
(Received 17 May 2009; published 2 September 2009)

The scaled static dipole polarizabilities of $1s$ and $2s$ states of hydrogenlike ions embedded in a plasma environment are calculated as function of the interaction screening. The plasma screening of Coulomb interaction is described by the Debye-Hückel potential. The electron energies and wave functions of bound and continuum states are calculated by solving numerically the Schrödinger equation with this potential in a symplectic integration scheme. The screening of Coulomb interactions reduces the number of bound states, decreases the energies of bound states and broadens the radial extension of the wave functions of bound and continuum states. All these effects result in a dramatic increase in static polarizability when the interaction screening increases. Comparison of present results with those of other authors is made when available.

DOI: 10.1103/PhysRevA.80.032502 PACS number(s): 32.10.Dk

I. INTRODUCTION

The effects of screened Coulomb interaction between charged particles in hot, dense plasmas on the atomic structure and collision properties have been subject to extensive studies in the last 30–40 years (see, e.g., [1,2] and references therein). These studies have been motivated mainly by the research in laser produced plasmas, extreme ultraviolet and x-ray laser development, inertial confinement fusion, and astrophysics (stellar atmospheres and interiors). The densities (n) and temperatures (T) in these plasmas span the ranges $n \sim 10^{15}-10^{18}$ cm^{-3}, $T \sim 0.5-5$ eV (stellar atmospheres), $n \sim 10^{19}-10^{21}$ cm^{-3}, $T \sim 50-300$ eV (laser plasmas), and $n \sim 10^{22}-10^{26}$ cm^{-3}, $T \sim 0.5-10$ keV (inertial confinement fusion plasmas). The Coulomb interaction screening in these plasmas is a collective effect of the correlated many-particle interactions and in the lowest particle correlation order (pairwise correlations) it reduces to the Debye-Hückel potential (for the interaction of an ion of charge Z with an electron) [1,2]

$$V(r) = -\frac{Ze^2}{r}\exp\left(-\frac{r}{D}\right), \tag{1}$$

where $D=(k_B T_e/4\pi e^2 n_e)^{1/2}$ is the Debye screening length, T_e and n_e are the plasma electron temperature and density, respectively, and k_B is the Boltzmann constant. The representation of charged particle interaction in a plasma by the potential Eq. (1) is adequate only if the Coulomb coupling parameter $\Gamma=e^2/(ak_B T_e)$ and plasma nonideality parameter $\gamma=e^2/(Dk_B T_e)$ satisfy the conditions $\Gamma \leq 1$, $\gamma \ll 1$, where $a=[3/(4\pi n_e)]^{1/3}$ is the average interparticle distance. There is, however, a wide class of laboratory and astrophysical plasmas in which these conditions are fulfilled (Debye plasmas). Expressions for the screened Coulomb interaction for strongly coupled and nonideal plasmas can be found elsewhere (see, e.g., [1,2]).

The polarizability is an important characteristic of an atomic system describing its response to an external electric field. It, therefore, describes the long-range dipole interaction of a charged particle with an atomic system and, thus, has an important role in collision processes involving such particles (see, e.g., [3,4]). For the isolated atoms and molecules, there exists a significant body of experimental and theoretical information on the static polarizabilities (see, e.g., [5]). However, for atomic systems embedded in a plasma environment where the Coulomb interaction is screened such information is virtually absent. The only work of this kind we are aware of is that of Saha *et al.* [6] in which the static polarizability of the ground-state hydrogen atom has been calculated by using the Debye-Hückel interaction Eq. (1) ($Z=1$). The eigenvalue problem in Ref. [6] was solved by the variational method employing a large Slater-type orbital (STO) basis for the discrete states. The continuum states (and their contribution to the polarizability) were not considered at all. These authors have found a significant increase in the static polarizability in the screened Coulomb potential with respect to the unscreened case. The values of polarizabilities for the $1s$ state of hydrogenlike ions in a Debye plasma calculated in the present work are even larger than those in Ref. [6] due to the inclusion of the contribution from transitions to continuum states (e.g., about twice larger for a Debye screening length of $D \simeq 2a_0$ than its value in the plasma free case, a_0 being the Bohr radius). Just like in the unscreened Coulomb interaction case, the interaction of a hydrogenlike ion (as a whole) with a charged structureless particle (e.g., electron, or bare nucleus) will be significantly affected by the dipole term of the multipole expansion of the interaction, the polarization interaction [3]. This will have a significant effect on the low-energy electron scattering (as described by the modified effective range theory [7]) but also on the low-energy heavy-particle collision processes (within their quasimolecular description [8]). The polarization interaction between the particles in Debye plasmas also affects the transport and thermodynamic properties of these plasmas [9].

In the present work we shall investigate the static polarizabilities of hydrogenlike ions in the $1s$ and $2s$ states with electron—nucleus interaction of Debye-Hückel type. We shall solve the Schrödinger equation in both the discrete and continuous spectrum of the potential Eq. (1) by employing the symplectic integration scheme [10,11]. This direct numerical integration method has been used also in our recent

investigations of photo excitation [12], photo ionization [13], and electron-impact excitation [14] processes in a Debye plasma. Compared with the variational method, the symplectic integration scheme should provide a more accurate solution of the eigenvalue problem with the potential Eq. (1). The inclusion of the continuum in the polarizability calculations is particularly important for the large screening parameters, $1/D$, when the electron binding energy is small and the coupling with the continuum is strong.

In the remaining part of the paper we shall use atomic units, unless otherwise is explicitly stated.

II. THEORETICAL CONSIDERATIONS AND COMPUTATIONAL METHOD

The static polarizability of an atomic system in the discrete quantum state $|n\rangle$ can be expressed, within the perturbation theory framework, as (see, e.g., [15])

$$\alpha = -2\sum_{k\neq n}\frac{|H_{nk}|^2}{E_n - E_k}, \tag{2}$$

where $H_{nk}=\langle\psi_n^{(0)}|\hat{z}|\psi_k^{(0)}\rangle$ is the dipole matrix element due to the presence of the external electric field oriented along the z direction, and $\psi_n^{(0)}, \psi_k^{(0)}$ and E_n, E_k are the wave functions and energies of unperturbed states $|nlm\rangle, |kl'm'\rangle$, respectively. It should be noted that $\psi_k^{(0)}$ in Eq. (2) denotes both a discrete and a continuum state; in the latter case the sum in Eq. (2) is replaced by an integral over the continuous variable $k=\sqrt{2\varepsilon}$, ε being the energy of the continuum state. For a central-symmetric potential, such as Eq. (1), the wave functions $\psi_n^{(0)}$ and $\psi_k^{(0)}$, as well known, can be represented in the form $\psi_n^{(0)}(\vec{r})=\frac{P_{nl}(r)}{r}Y_{lm}(\theta,\phi)$ (and similarly for $\psi_k^{(0)}$), that transforms the expression (2) into

$$\alpha = -\frac{2}{3}\sum_{k\neq n}\frac{|R_{nk}|^2}{E_n - E_k} \tag{3}$$

with $R_{nk}=\langle P_{nl}|r|P_{kl'}\rangle$. The calculation of the static polarizability of a hydrogenlike ion in the state $|n\rangle$ in a Debye plasma is thus reduced to solving the radial Schrödinger equation with the potential Eq. (1) in the discrete and continuous spectrum, calculation of corresponding dipole matrix elements and performing the summation Eq. (3) over the discrete and continuum spectrum [in the latter case Eq. (3) is replaced by an integral].

The eigenvalue problem in the Debye-Hückel potential Eq. (1) has certain features that significantly change both the structure of Eq. (3) and the value of the polarizability with respect to the unscreened Coulomb case. As well known [16], for any finite value of the Debye length D the potential Eq. (1) supports only a finite number of bound states. With decreasing the value of D (increasing the screening), the binding energy of a given discrete state decreases and at a certain critical value of D it merges with the continuum edge. This implies that with decreasing D, the number of bound states in the potential decreases thus reducing the sum Eq. (3) over the discrete spectrum to a smaller and smaller number of terms. This is in sharp contrast with the unscreened Coulomb case where the sum Eq. (3) over the discrete spectrum includes an infinite number of terms. Another important feature of the screened Coulomb potential is that the energy levels are not anymore degenerate with respect to the orbital angular momentum l. The lifting of l degeneracy of energy levels in the potential Eq. (1) also affects the structure of Eq. (3).

As mentioned in the Introduction, we shall solve the radial Schrödinger equation with the potential Eq. (1) in both the discrete and continuous energy spectrum by the symplectic integration method. The details of this direct numerical integration method, as implemented to the radial Schrödinger equation with the potential Eq. (1), are given in Refs. [12–14] and will not be repeated here. We only mention that the accuracy with which the method has been implemented in the present calculations is 10^{-7} for the eigenenergies E_{nl} and 10^{-5} for the wave functions. We further mention that the radial Schrödinger equation with the potential Eq. (1) after the scaling transformation

$$\rho = Zr, \quad \delta = ZD, \quad \varepsilon_{\kappa l}(\delta) = E_{\kappa l}(Z,D)/Z^2, \tag{4}$$

is reduced to that for the hydrogen atom ($Z=1$) in the potential Eq. (1)

$$\left(-\frac{d^2}{2d\rho^2} + \frac{l(l+1)}{2\rho^2} - \frac{\exp(-\rho/\delta)}{\rho}\right)P_{\kappa l}(\rho;\delta) = \varepsilon_{\kappa l}(\delta)P_{\kappa l}(\rho;\delta) \tag{5}$$

where $\kappa=n$ for the discrete states and $\kappa=k(=\sqrt{2\varepsilon})$ for the continuum states. Equation (5) is to be solved with the appropriate boundary conditions [12–14]. The radial wave functions of discrete states are orthonormalized in the conventional way, while those of the continuum (from now on we denote them by $P_{\varepsilon l}$) are normalized to unit energy interval ε (see, e.g., [16]). From the scaling relations Eq. (4) and the normalization conditions for the wave functions, the following scaling relations for the dipole matrix elements derive [12,14].

For the bound-bound transitions

$$\langle P_{nl}(r;Z,D)|r|P_{n'l'}(r;Z,D)\rangle = Z^{-1}\langle P_{nl}(\rho;\delta)|\rho|P_{n'l'}(\rho;\delta)\rangle. \tag{6}$$

For the bound-free transitions

$$\langle P_{nl}(r;Z,D)|r|P_{\varepsilon l'}(r;Z,D)\rangle = Z^{-2}\langle P_{nl}(\rho;\delta)|\rho|P_{\varepsilon l'}(\rho;\delta)\rangle. \tag{7}$$

From the relations Eqs. (3), (4), (6), and (7), it follows that the static dipole polarizability $\alpha_{nl}(Z,D)$ of the hydrogenlike ion in a state nl embedded in a Debye plasma scales as

$$\alpha_{nl}(Z,D) = Z^{-4}\alpha_{nl}(\delta). \tag{8}$$

In the present work we consider the polarizability of hydrogenlike ions in the states $nl=1s$ and $nl=2s$. In order to reveal the factors that influence the changes in the dipole polarizability due to the interaction screening, we shall consider the $nl=1s$ case in more detail. In the next section we analyze the behavior of the bound and continuum wave func-

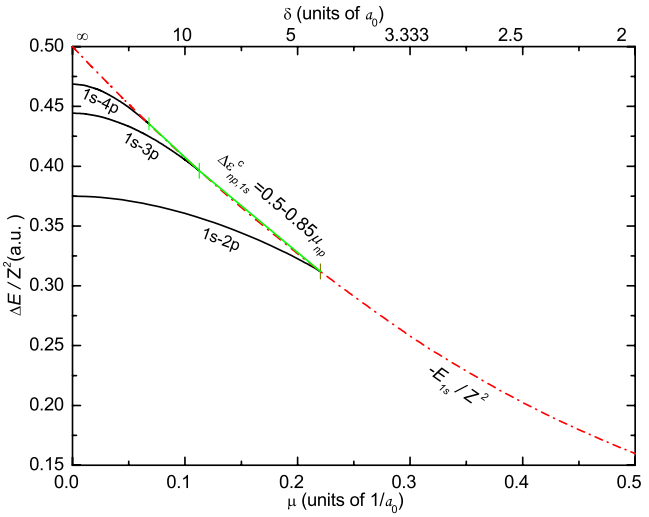

FIG. 1. (Color online) Scaled energy differences between the $1s$ and np ($n \leq 4$) states of hydrogenlike ions as function of scaled screening parameter μ. The scaled energy of $1s$ state is also shown.

tions, dipole matrix elements and the transition energies when the interaction screening parameter $\mu = 1/\delta$ varies.

III. SCALED ENERGIES, WAVE FUNCTIONS, AND DIPOLE MATRIX ELEMENTS

For the calculation of $\alpha_{1s}(\delta)$ static polarizability, the behavior on μ (or δ) of the energy differences between the np and $1s$ states are relevant for the discrete part of Eq. (3), as well as the μ dependence of the energy of $1s$ state [for the continuum part of Eq. (3)]. In Fig. 1 we show the scaled energy $-\varepsilon_{1s} = -E_{1s}/Z^2$ and the energy differences (transition energies) $\Delta\varepsilon_{np,1s} = (E_{np} - E_{1s})/Z^2$ between the $1s$ and np ($n \leq 4$) states as function of the scaled screening parameter $\mu = 1/\delta$. With increasing the plasma screening, both $-\varepsilon_{1s}(\mu)$ and $\Delta\varepsilon_{np,1s}(\mu)$ rapidly decrease. [We should note that the energy difference $\Delta\varepsilon_{\varepsilon p,1s}(\mu) = \varepsilon_{\varepsilon p} - \varepsilon_{1s}(\mu)$, where $\varepsilon_{\varepsilon p}$ is the constant energy of a continuum state, will obviously also exhibit a rapid decrease.] For a given np state, the function $\Delta\varepsilon_{np,1s}(\mu)$ terminates at $\mu^c_{np} = 1/\delta^c_{np}$, the critical screening parameter at which the np bound state merges with the continuum edge. The values of critical Debye lengths for the $1s$, $2p$, $3p$, and $4p$ states are: $\delta^c_{1s} = 0.839908 a_0$, $\delta^c_{2p} = 4.541 a_0$, $\delta^c_{3p} = 8.872 a_0$, $\delta^c_{4p} = 14.74 a_0$. It is interesting to observe that the ending values, $\Delta\varepsilon^c_{np,1s}$ of transition energies as function of μ, lie on the line $\Delta\varepsilon^c_{np,1s}(\text{a.u.}) = 0.5 - 0.85\mu^c_{np}$. (Obviously, for $\mu \to 0$ and $n \to \infty$, $\Delta\varepsilon^c_{np,1s}(\text{a.u.}) = 0.5$). The decrease in energy differences $\Delta\varepsilon_{np,1s}(\mu)$ and $\Delta\varepsilon_{\varepsilon p,1s}(\mu)$ with increasing μ obviously leads to an increase in the polarizability $\alpha_{1s}(\delta)$ when the interaction screening increases.

In Figs. 2(a)–2(c) we show, respectively, the scaled wave functions $P_{nl}(\rho)$ of the $1s$, $2p$, and $3p$ states for a number of the screening lengths δ and for the unscreened case. With the decrease in δ, the radial extension of the bound-state wave functions increases significantly, its peak and node (in the case of $3p$) are shifted toward the larger radial distances and the peak magnitude decreases. All these features are particularly pronounced when the Debye length for a given nl state approaches its critical value δ^c_{nl} (see above). This behavior of the radial wave functions with decreasing δ decreases their overlap and, thereby, the dipole coupling between $1s$ and np discrete states. On the other hand, the enhanced radial spread of the bound-state wave functions with decreasing δ increases their overlap with the continuum states and thereby

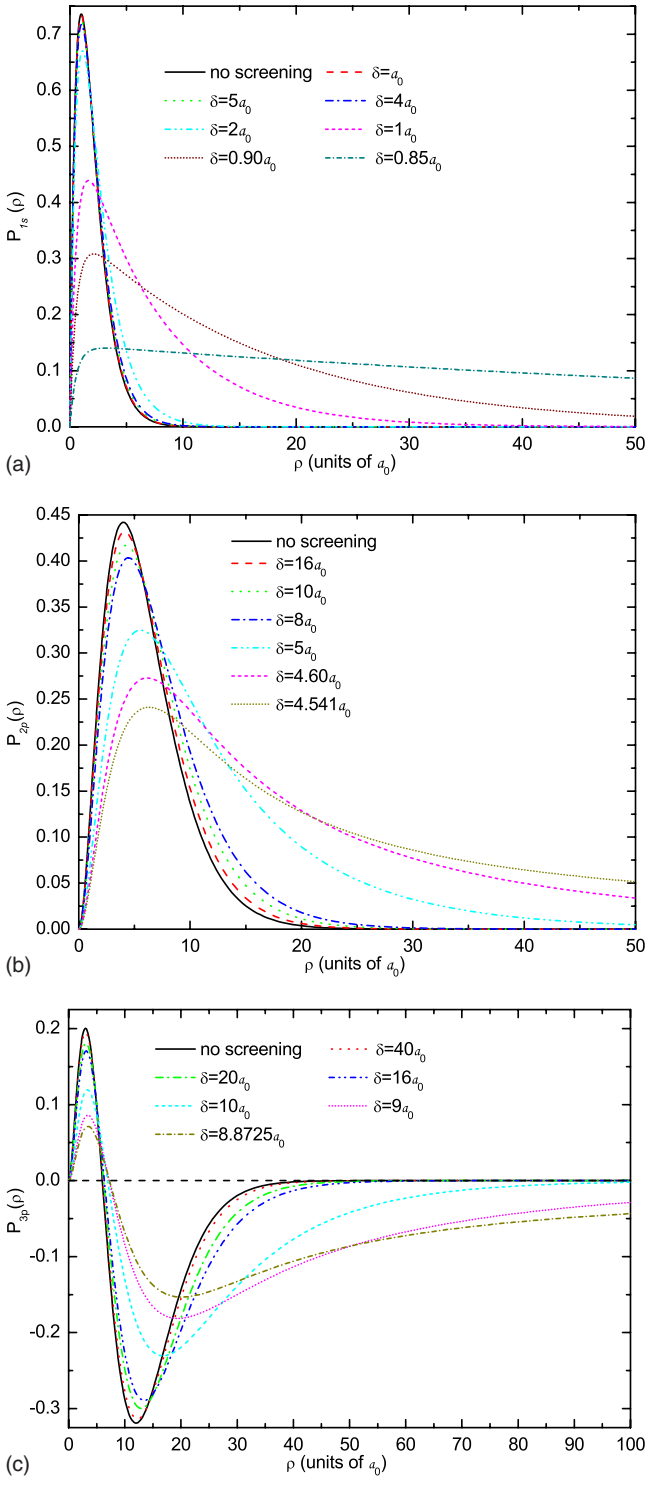

FIG. 2. (Color online) Radial wave functions of the $1s$ (a), $2p$ (b), and $3p$ (c) bound states for a number of screening lengths δ and for the unscreened case.

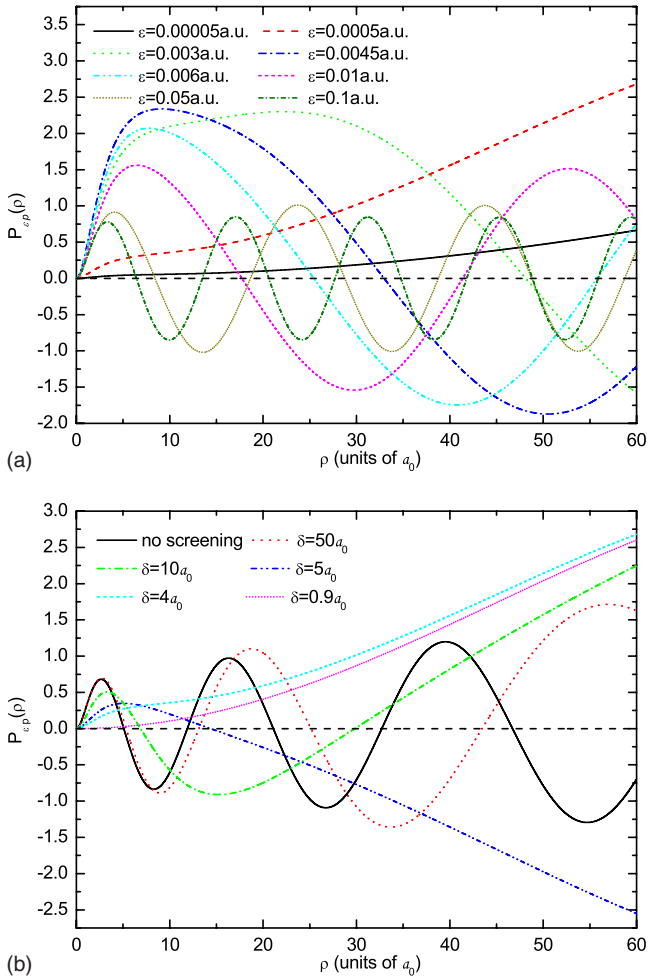

FIG. 3. (Color online) Continuum wave functions for a number of scaled screening lengths δ and scaled electron energies ε. Panel (a): fixed scaled screening length $\delta=4a_0$; panel (b): fixed scaled electron energy $\varepsilon=0.0005$ a.u.

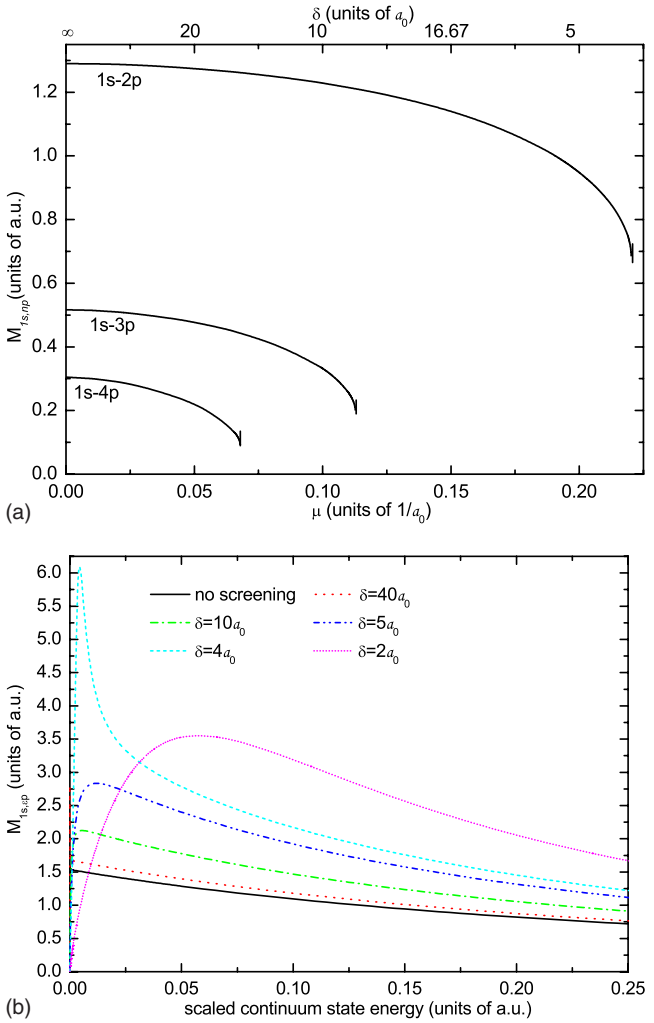

FIG. 4. (Color online) (a) Scaled dipole matrix elements between the $1s$ and $np(n\leq 4)$ states as function of the screening parameter $\mu=1/\delta$; (b) scaled dipole matrix element between the $1s$ and the continuum state εp states as function of scaled continuum state energy for a number of screening lengths δ.

the coupling with the continuum. These consequences of the behavior of the bound state wave functions with varying δ will become evident in the discussion of dipole matrix elements [see below, Fig. 4(a)].

The energy-normalized continuum p-wave functions for a fixed value $\delta=4a_0$ of Debye length and a number of continuum energies are shown in Fig. 3(a), while the p-wave functions for a fixed energy $\varepsilon=0.0005$ a.u. and a number of screening lengths are shown in Fig. 3(b). In both cases, the continuum wave functions exhibit strong changes in their oscillation frequencies and amplitudes when varying one of these parameters. For the $\delta=4a_0$ case [Fig. 3(a)] the frequency decreases and the amplitude increases with decreasing the energy of the state. For the $\varepsilon=0.0005$ a.u. case [Fig. 3(b)], again the frequency decreases and the amplitude increases when the screening length decreases. In both of these cases the amplitude of the oscillations increases with increasing the radial distance. This behavior of the continuum wave functions with varying the energy of continuum electron and the Debye screening length is reflected in the behavior of the $1s$-εp dipole matrix elements [see below, Fig. 4(b)].

The scaled dipole matrix elements $M_{1s,np}$ for the $1s$-np $(n=2-4)$ transitions as function of screening parameter $\mu=1/\delta$ are shown in Fig. 4(a). They first decrease monotonically with the increase in μ, but their decrease becomes very sharp when μ approaches the corresponding critical value $\mu_{np}^c=1/\delta_{np}^c$. As argued earlier, the sharp decrease in $M_{1s,np}$ matrix element when μ approaches μ_{np}^c is due to the large spread of the np—wave function outside the region of radial distances within which the $1s$—wave function is still dominantly confined (i.e., the overlap of the two wave functions is small). For a given value of μ, the $M_{1s,np}$ matrix elements rapidly decrease with increasing n. It should be remarked that the simultaneous decrease in the transition energies and the $M_{1s,np}$ matrix elements with increasing μ leaves the question of the effect of their simultaneous variation on the value of polarizability remains open before calculating their ratio as it appears in Eq. (3). As we shall see in the next section, the decrease in $M_{1s,np}$ with increasing μ is faster than the decrease in $\Delta\varepsilon_{np,1s}(\mu)$.

Figure 4(b) gives the scaled dipole matrix element $M_{1s,\varepsilon p}$ for the $1s$-εp transition as function of the energy of con-

TABLE I. Scaled ground-state energies, transition energies, and oscillator strengths of hydrogenlike ions for various screening lengths, δ.

	$-\varepsilon_{1s}$ (a.u.)			Transition energy (a.u.)		Oscillator strength	
$\delta(a_0)$	a	b	Transition	a	b	a	b
∞	0.5000	0.5000	$1s\rightarrow 2p$	0.37500	0.37500	0.4160	0.4162
			$1s\rightarrow 3p$	0.44444	0.44444	0.0790	0.0791
			$1s\rightarrow 4p$	0.46875	0.46875	0.0290	0.0290
20	0.45182	0.45182	$1s\rightarrow 2p$	0.37107	0.37108	0.4000	0.40175
			$1s\rightarrow 3p$	0.43325	0.43326	0.0660	0.06585
			$1s\rightarrow 4p$	0.44922	0.44922	0.0150	0.01448
10	0.40705	0.40706	$1s\rightarrow 2p$	0.36051	0.36052	0.3561	0.3630
			$1s\rightarrow 3p$	0.40546	0.40547	0.0298	0.0298
5	0.32674	0.32681	$1s\rightarrow 2p$	0.32263	0.32271	0.1773	0.1933
4	0.29076	0.29092	$1s\rightarrow 2p$	0.29479		0.0383	
1	–0.16598	0.01029	$1s\rightarrow 2p$	0.01907		0.0034	

[a]Data from Ref. [6].
[b]Present data.

tinuum state for a number of scaled screening lengths. The $M_{1s,\varepsilon p}$ matrix elements generally decrease with increasing the energy of continuum state and increase with decreasing the screening length. This is consistent with the general behavior of the continuum wave functions observed in Figs. 3(a) and 3(b). However, the $M_{1s,\varepsilon p}$ matrix elements in the screened interaction case exhibit maxima in the low-energy region and diminish when the energy of continuum state tends to zero. This behavior can be anticipated already from Fig. 3(a) where the wave function for the energy of 0.00005 a.u. and $\delta=4a_0$ is very small up to distances of $20a_0$, while the radial distribution of $1s$ wave function for $\delta=4a_0$ is negligible already beyond $10a_0$ [see Fig. 2(a)].

Figures 4(a) and 4(b) show that with decreasing δ, the $M_{1s,np}$ matrix elements decrease, while the integrals over the energy of $M_{1s,\varepsilon p}$ matrix elements increase. These changes are particularly pronounced when δ approaches its critical value δ_{np}^c. This indicates that the contribution of continuum states to the dipole polarizability increases with decreasing δ. It becomes the only contribution to the polarizability α_{1s} when all bound np states are merged with the continuum (i.e., for $\delta<\delta_{2p}^c=4.541a_0$).

IV. STATIC POLARIZABILITIES OF HYDROGENLIKE IONS IN 1*s* AND 2*s* STATES

In this section we present the results of our calculations for the scaled polarizabilities of hydrogenlike ions in their $1s$ and $2s$ states, performed by using Eq. (3). We note that the energy of $2s$ state for finite values of δ lies below the energy of $2p$ state [17,18] and that $\delta_{2s}^c=3.223a_0$. When calculating the sum Eq. (3) over the discrete spectrum, we have included all the np states that for a given value of the screening length remain bound. The integration over the continuum energies was performed with a variable step in order to ensure the numerical accuracy.

We first present the results for the polarizabilty of $1s$ state for which comparison for a number of values of δ is possible with the results of Ref. [6]. As mentioned in the introduction, the eigenfunctions and eigenenergies in the potential Eq. (1) were determined in Ref. [6] by using the variational method with an STO basis but only in the discrete spectrum. In Table I we compare the ground state energies, as well as the transition energies and oscillator strengths for $1s$-np transitions for a number of screening lengths obtained in the present work and in Ref. [6]. While the ground state and transition energies of the variational method agree quite well with the present results down to screened lengths of $4a_0$ and $5a_0$, respectively, the differences in the oscillator strengths become significant already for $\delta=20a_0$ (particularly for higher np states). It is important to note that in variational calculations of Ref. [6] the $2p$ state is still bound for $\delta=4a_0$, contrary to the present result (and those of others, [17,18]) that this state enters the continuum at $\delta_{2p}^c=4.541a_0$. A further indication that the variational method employed in Ref. [6] fails to adequately describe the electronic state when its energy approaches the continuum edge is that the ground-state energy at $\delta=1a_0$ becomes positive (see Table I), while this energy becomes zero only at $\delta_{1s}^c=0.839908a_0$.

In Table II we show the scaled dipole polarizabilities for the $1s$ state of hydrogenlike ions for a number of screening lengths. The contributions of the $2p$, $3p$, and $4p$ states and of the continuum to the polarizability are also given in this table. The values of α_{1s} from Ref. [6] available for a number of screening lengths (and for the unscreened case) are also shown in the table. It should be noted that for $\delta\leq 5a_0$ the continuum contribution to the polarizability becomes dominant, and for $\delta\leq 4a_0$ (more correctly, for $\delta<\delta_{2p}^c=4.541a_0$) it is the exclusive contributor to the polarizability. The values of Ref. [6] for $\delta=5a_0$, $4a_0$ and $1a_0$ should be considered as lying within the uncertainties of the applied method when the energies of bound states are close to the continuum and due to the complete exclusion of the continuum contribution to the polarizability.

TABLE II. Scaled static dipole polarizabilities α_{1s}/Z^4 of the ground-state hydrogenlike ion for a number of scaled screening lengths, δ.

		Contributions			
$\delta(a_0)$	Polarizability	$2p$	$3p$	$4p$	Continuum
∞	4.5000 (4.4997)[a]	2.95962	0.40045	0.13194	0.83878
50	4.50820	2.95195	0.39154	0.12072	0.97086
40	4.51299	2.94814	0.38685	0.11513	1.00813
20	4.55176 (4.5412)[a]	2.91784	0.35053	0.07174	1.21164
16	4.58003	2.89524	0.32349	0.03779	1.32351
10	4.69933 (4.6577)[a]	2.79236	0.18149		1.72548
5	5.27661 (5.0936)[a]	1.85622			3.42039
4	5.72635 (5.41)[a]				5.72635
3	6.80156				6.80156
2	11.14701				11.14701
1.9	12.3359				12.3359
1.7	16.0699				16.0699
1.5	24.0987				24.0987
1.3	47.4052				47.4052
1.2	82.9946				82.9946
1.1	192.910				192.910
1.08	244.785				244.785
1.06	316.994				316.994
1.04	409.154				409.154
1.02	598.717				598.717
1	788.280 (8.23)[a]				788.280

[a]Data from Ref. [6].

From Table II one can observe that the relative increase in the continuum contribution to the polarizabilty with decreasing δ is larger than the increase in total polarizability in the region of δ where the discrete spectrum contributes to α_{1s} (i.e., for $\delta > 4.541a_0$). Subtracting from α_{1s} in this region the continuum contribution, we see that the contribution of the discrete spectrum to the polarizability in fact decreases with decreasing δ. Therefore, the enhanced coupling with the continuum of the $1s$ state is the only factor that causes the increase in α_{1s} polarizability when δ decreases.

The variation in scaled polarizability α_{1s} as function of screening parameter μ is shown in Fig. 5. When $\mu \to \mu_{1s}^c = 1/\delta_{1s}^c = 1.1906066 a_0^{-1}$ the polarizability attains values of the

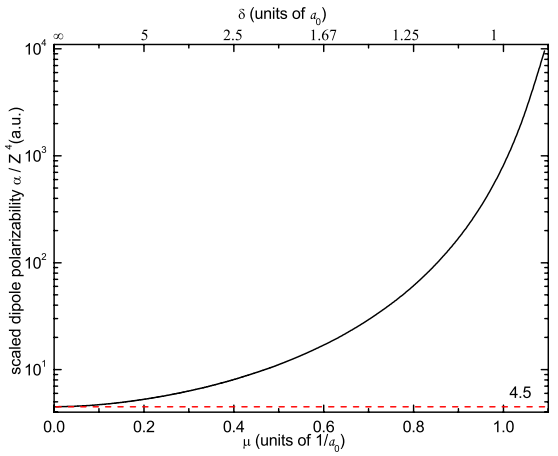

FIG. 5. (Color online) Scaled dipole polarizability of the ground state hydrogenlike ions as function of the scaled screening parameter μ. (The limiting $\mu=0$ value of 4.5 a.u. is the polarizability in the pure Coulomb case.)

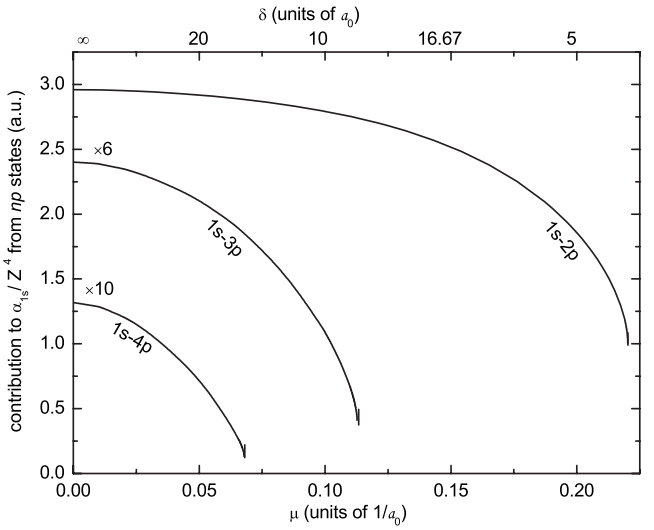

FIG. 6. Contributions to the scaled polarizability from the individual $np(n \leq 4)$ states as function of scaled screening parameter μ.

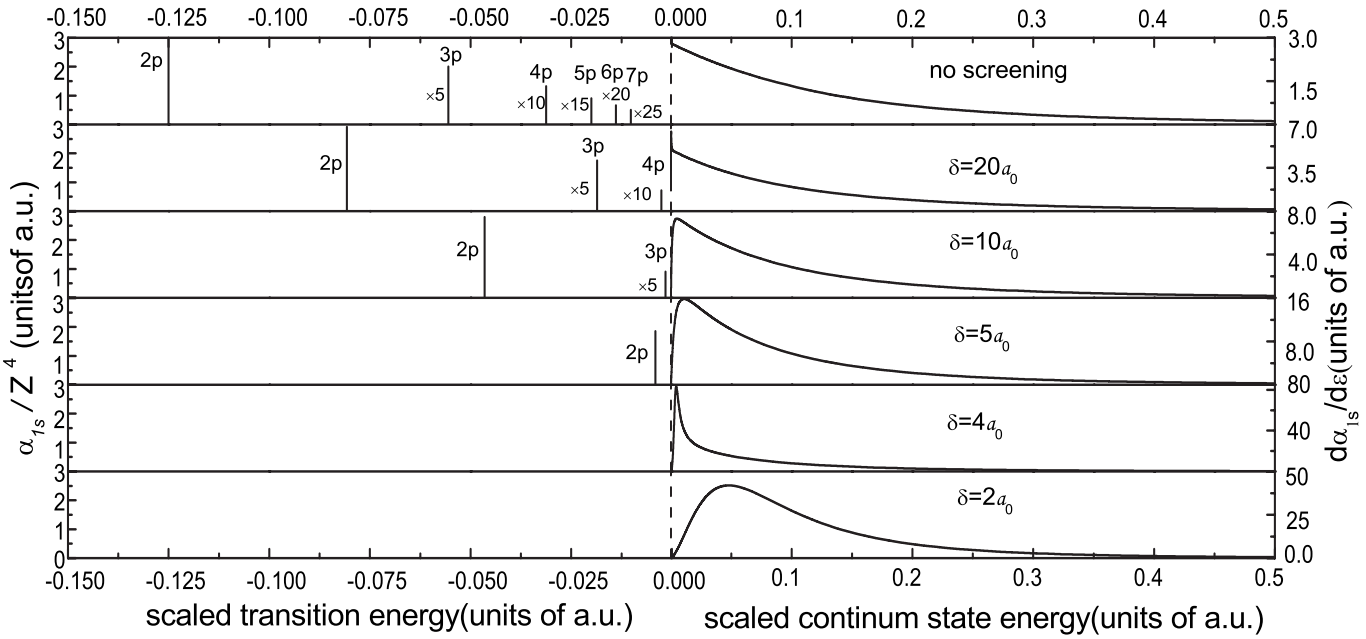

FIG. 7. Contributions to the scaled polarizability from individual bound and continuum states for hydrogenlike ions for the unscreened and screened cases with a number of screening lengths. (Note the change of the scale on the right-hand-side of the figure for $d\alpha/d\varepsilon$ for different values of δ.)

order of 10^4, but at $\mu=\mu_{1s}^c$ it loses its physical meaning since the electron is already in the continuum. The dramatic increase in the polarizability when $\mu\to\mu_{1s}^c$ is a mere result of the strong overlap of bound-state wave function with the continuum. As seen in Fig. 5, the calculated scaled polarizability in the limit $\mu\to 0$ has the correct value of 4.5 a.u. [5].

The contributions to the scaled α_{1s} polarizability from $2p$, $3p$, and $4p$ states as function of screening parameter μ are shown in Fig. 6, while the differential contribution of the continuum for a number of screening lengths is shown in Fig. 7 as function of transition energy, ε. On the left side of Fig. 7 ($\varepsilon<0$) shown are also (by vertical lines) the contributions from the transitions from $1s$ to the bound np states remaining in the discrete spectrum for a given δ (indicated in each panel). The heights of vertical lines on Fig. 7 correspond to the values of α_{1s} in Table II for a given state and δ. It is seen from this figure that with decreasing δ less and less discrete np states contribute to the α_{1s} polarizability as they successively enter into the continuum at their respective critical screening lengths. For $\delta=5$ only the $2p$ state remains in the discrete spectrum and for $\delta<\delta_{2p}^c=4.541a_0$ only the transitions to continuum states contribute to α_{1s}. The variations in these contributions with the corresponding parameter are quite similar to the variations of $M_{1s,np}$ and $M_{1s,\varepsilon p}$ matrix elements in Figs. 4(a) and 4(b), respectively.

We now turn to the results of calculations of the polarizability α_{2s}. The calculations of α_{2s} by using the perturbation formula (2), valid for nondegenerate states, could be performed only for $\delta\leq 7a_0$. For $\delta>7a_0$ the energy difference between the $2s$ and $2p$ states becomes comparable to or smaller than the values of corresponding matrix elements (squared) and the perturbation approach for calculation of α_{2s} becomes inappropriate. Instead, the variational [19] and Green's function [20,21] methods have to be employed in such cases (degenerate or quasidegenerate states). The results for α_{2s}, together with the energies of $2s$ and $2p$ states for a selected set of screening lengths are shown in Table III. As expected, the α_{2s} polarizability is much larger than α_{1s} for the same value of the screening length (compare the values in Tables II and III). The gradual increase in α_{2s} down to $\delta=5.5a_0$ is mainly due to $2s$-$2p$, $3p$, transitions, while for $\delta\leq 5a_0$ the continuum contribution to α_{2s} starts to dominate. For $\delta\leq 4.541a_0$, the continuum is the only contributor to α_{2s}. When $\delta\to\delta_{2s}^c=3.223a_0$, α_{2s} increases dramatically, reaching the value of 7.893×10^5 already at $\delta=3.4a_0$. We note that the static polarizability of hydrogen atom in its $2s$ state in the plasma free case is $120a_0^3$ [19–21].

TABLE III. Scaled energies of $2s$ and $2p$ states and scaled static dipole polarizability of hydrogenlike ions in the $2s$ state for a number of scaled screening lengths, $\delta=ZD$. Numbers in parentheses indicate powers of 10.

$\delta(a_0)$	7	6	5.8	5.5	5	4.6	4.2	4	3.8	3.6	3.4
$-E_{2s}/Z^2$(a.u.)	0.05994	0.04281	0.03917	0.03361	0.02422	0.01681	9.889(−3)	6.792(−3)	4.079(−3)	1.903(−3)	2.293(−4)
$-E_{2p}/Z^2$(a.u.)	0.04845	0.02897	0.02483	0.01855	0.0082	8.515(−4)					
α_{2s}/Z^4(a.u.)	2.651(3)	2.691(3)	2.747(3)	2.882(3)	3.347(3)	4.248(3)	1.310(4)	2.021(4)	3.990(4)	1.296(5)	7.893(5)

V. CONCLUSIONS

In the present paper we have investigated the effects of Debye-Hückel screening of the Coulomb interaction on the static dipole polarizabilities α_{1s} and α_{2s} of hydrogenlike ions in $1s$ and $2s$ states, respectively. We have found that both the energy differences and dipole matrix elements entering the expression (3) for the static polarizability decrease when the Debye screening length δ decreases, the decrease being very sharp when the screening length approaches its critical value δ_{nl}^c. In contrast, the dipole matrix elements with the continuum states increase with decreasing δ except in the near-threshold region. The overall effect of these changes is that the contribution of the discrete part of the spectrum to the polarizability (which includes all the states that remain bound for a given value of δ) decreases with decreasing δ, while the contribution of the continuum states increases. As a result, both α_{1s} and α_{2s} gradually increase when δ decreases down to $\delta=\delta_{2p}^c=4.541a_0$, the screening length at which the $2p$ state enters the continuum, followed by a dramatic increase when $\delta\rightarrow\delta_{1s}^c=0.839908a_0$ and $\delta\rightarrow\delta_{2s}^c=3.223a_0$, respectively, due to the strong overlap of $1s$ and $2s$ wave functions with the continuum in these regions of δ.

ACKNOWLEDGMENTS

One of us (R.K.J.) is grateful to the Institute of Applied Physics and Computational Mathematics, Beijing, for the warm hospitality during the period when this work was performed. This work has been partly supported by the National Natural Science Foundation of China (Grants No. 10604011, No. 10734140, and No. 10875017) and the National Key Laboratory of Computational Physics Foundation (No. 9140C6904030808).

[1] D. Salzman, *Atomic Physics in Hot Plasmas* (Oxford Univ. Press, Oxford, 1998).
[2] M. S. Murillo and J. C. Weisheit, Phys. Rep. **302**, 1 (1998).
[3] T. M. Miller and B. Bederson, Adv. At. Mol. Phys. **13**, 1 (1978).
[4] X. Chu, A. Dalgarno, and G. C. Groenenboom, Phys. Rev. A **75**, 032723 (2007).
[5] T. M. Miller, *Atomic and Molecular Polarizabilities* (CRC Press, Boca Raton, FL, 1995), Vol. 75.
[6] B. Saha, P. K. Mukherjee, and G. H. F. Diercksen, Astron. Astrophys. **396**, 337 (2002).
[7] T. F. O'Malley, L. Rosenberg, and L. Spruch, Phys. Rev. **125**, 1300 (1962).
[8] B. H. Bransden and M. R. C. McDowell, *Charge Exchange and the Theory of Ion-Atom Collisions* (Clarendon, Oxford, 1992).
[9] T. S. Ramazanov, K. N. Dzumagulova, Yu. A. Omarbakiyeva, and G. Röpke, J. Phys. A **39**, 4369 (2006).
[10] E. Forest and R. D. Ruth, Physica D **43**, 105 (1990); H. Yoshida, Phys. Lett. A **150**, 262 (1990).
[11] X. S. Liu, X. Y. Liu, Z. Y. Zhou, P. Z. Ling, and S. F. Pan, Int. J. Quantum Chem. **79**, 343 (2000).
[12] Y. Y. Qi, J. G. Wang, and R. K. Janev, Phys. Rev. A **78**, 062511 (2008).
[13] Y. Y. Qi, Y. Wu, and J. G. Wang, Phys. Plasmas **16**, 033507 (2009).
[14] Y. Y. Qi, Y. Wu, J. G. Wang, and Y. Z. Qu, Phys. Plasmas **16**, 023502 (2009).
[15] R. W. Cowan, *The Theory of Atomic Structure and Spectra* (University of California Press, Berkeley, 1981).
[16] L. D. Landau and E. M. Lifshitz, *Quantum Mechanics: Non-Relativistic Theory* (Pergamon, London, 1958).
[17] F. J. Rogers, H. C. Graboske, and D. J. Harwood, Phys. Rev. A **1**, 1577 (1970).
[18] L. Liu, J. G. Wang, and R. K. Janev, Phys. Rev. A **77**, 032709 (2008).
[19] M. N. Adamov, M. D. Balmakov, and T. K. Rebane, Opt. Spektrosk. **27**, 100 (1969) [Opt. Spectrosc. **27**, 100 (1969).]
[20] B. J. Laurenzi, D. G. Williams, and G. S. Batia, J. Chem. Phys. **61**, 2077 (1974).
[21] H. K. McDowell and R. N. Porter, J. Chem. Phys. **65**, 658 (1976).